

# Influence of natural dye adsorption on the structural, morphological and optical properties of TiO<sub>2</sub> based photoanode of dye-sensitized solar cell

M. KHALID HOSSAIN<sup>1</sup>, M.F. PERVEZ<sup>1</sup>, M. JALAL UDDIN<sup>2</sup>, S. TAYYABA<sup>3</sup>, M.N.H. MIA<sup>1</sup>, M.S. BASHAR<sup>4</sup>, M.K.H. JEWEL<sup>2</sup>, M.A.S. HAQUE<sup>1</sup>, M.A. HAKIM<sup>5</sup>, MUBARAK A. KHAN<sup>1,\*</sup>

<sup>1</sup>Atomic Energy Research Establishment, Bangladesh Atomic Energy Commission, Dhaka-1349, Bangladesh

<sup>2</sup>Dept of AECE, Islamic University, Kushtia-7003, Bangladesh

<sup>3</sup>Department of Computer Engineering, The University of Lahore, Lahore-54000, Pakistan

<sup>4</sup>Institute of Fuel Research and Development, BCSIR, Dhaka-1205, Bangladesh

<sup>5</sup>Department of GCE, Bangladesh University of Engineering and Technology, Dhaka-1000, Bangladesh

Porous photoanodes of dye-sensitized solar cells (DSSCs) can adsorb specific type of natural or organic dyes. Adsorption of the dye results in a change of the structural, morphological and optical characteristics of the photoanode. In this work, we present a comparative study on the adsorption effect of natural dye (*Curcuma Longa sp.*) on the structural, morphological and optical properties of mesoporous titanium dioxide (TiO<sub>2</sub>) photoanode on indium tin oxide (ITO) coated glass. A number of investigations including XRD, UV-Vis spectroscopy, EDS, and SEM were carried out to observe the variations due to adsorbed dye on TiO<sub>2</sub> surface. XRD characterization revealed the effect of dye adsorption on specific surface area (SSA), crystallite size, and morphological index (MI). In this case, increasing SSA with decreasing particle size was found for both dye adsorbed and dye free DSSC photoanode samples. Also, the MI and SSA were found to be directly and inversely proportional to the crystallite size respectively. UV-Vis-NIR spectroscopy showed that dye adsorption changes the light absorption, transmittance, and optical bandgap of the photoanode. Average atomic mass percentage of titanium (Ti) and oxygen (O) obtained from EDS analysis proved the presence of TiO<sub>2</sub> in the mesoporous photoanode. In SEM images, significant morphological changes of mesoporous TiO<sub>2</sub> surface appeared because of dye adsorption.

Keywords: natural dye; XRD analysis; TiO<sub>2</sub> photoanode surface morphology; UV-Vis-NIR; optical bandgap

## 1. Introduction

Dye sensitized solar cell (DSSC), a promising alternative candidate to p-n junctions solar cell [1–5], is fabricated based on sensitization of wide band gap semiconductor materials [6, 7]. In DSSC device, wide bandgap semiconductors such as SnO<sub>2</sub>, TiO<sub>2</sub> or ZnO are used due to their high chemical stability [7–9]. DSSC contributes more or less, along with other organic and inorganic photovoltaic (PV) technologies, to meet the world's energy crisis, in addition to the conventional fossil or natural gas based energy supplies. Since the first invention of DSSC by O'Regan et al. [10], it

has attracted extensive research focus as a novel renewable and clean photon-to-electricity conversion system. DSSCs facilitate its fabrication by cost-effective and commercially available materials eliminating the need of highly well-trained hands as well as elaborative and expensive laboratory setup [1, 7, 11].

Working mechanism of DSSCs is quite different than other conventional semiconductor PV devices. Usually, sensitizer in DSSC absorbs solar energy to generate excitons [12, 13] followed by capturing the exciton originated electrons by a wide band gap semiconductor photoanode film [14, 15]. A redox couple (e.g. I<sub>3</sub><sup>-</sup>/I<sup>-</sup> in an organic solvent), which fills the gap between the two electrodes of the DSSC, i.e. photo-electrode (photoanode) and

\*E-mail: makhan.inst@gmail.com

counter (working) electrode [10, 16–19], transports the charge carriers from metal oxide and oxidized dye to electrodes [20, 21].

The acceptor materials and dye sensitizers are the key constituents that regulate the performance of DSSC [22, 23]. Best efficiency obtained so far for silyl-anchor and carboxy-anchor dyes based DSSC is 14.7 % [24], which is 12.3 % with cobalt-based redox mediators [25, 26]. These achievements of DSSCs open manyfold doors for researching on alternative dyes with some more effective redox mediators and metal complexes in optimized semiconductor film for the further improvement of DSSC efficiencies.

In DSSC, using synthetic dyes as photosensitizer is very challenging due to the long-time dye preparation procedure, complexity of dye purification, and finding appropriate solvents for the dye extraction. As a result, commercial production of effective synthetic dyes for DSSC is still very expensive for photoanode development [27]. TiO<sub>2</sub> based photoanode can adsorb most of the available dyes which are commonly used as a sensitizer [28–30]. Therefore, natural dyes in TiO<sub>2</sub> based DSSC devices would be potential candidates in solving current photoanode development problems [31–33].

When dye is adsorbed on a photoanode surface, changes occur between the dye and the coating layer of the photoanode. Turmeric (*Curcuma Longa sp.*) has already been suggested as a promising dye to be used in DSSC by several groups [34–37]. The impact of photovoltaic response and sensitization time on photovoltaic performance of DSSCs using solvents extracted turmeric (*Curcuma Longa sp.*) natural dye had already been studied [34]. However, the influence of turmeric natural dye adsorption onto TiO<sub>2</sub> based DSSC's photoanode on structural, morphological and optical properties has been rarely found in the literature surveys, to the best of our knowledge.

In this experiment, we developed natural dye (*Curcuma Longa sp.*) adsorbed titanium dioxide (TiO<sub>2</sub>) photoanode by doctor blade method using an established recipe with different compositions

of constituent chemicals. The reason behind using *Curcuma Longa sp.* as a dye is that it is locally available, cost-effective and easy for dye pigment separation. The developed photoanodes surfaces have been studied by using XRD, UV-Vis-NIR spectroscopy, EDS and SEM to investigate structural properties (crystallite size, morphology index, specific surface area), optical properties (optical bandgap, absorption coefficient), and surface morphology of dye free and dye adsorbed photoanodes. The SEM image of the dye free photoanode shows mesoporous properties, whereas the mesopores of dye adsorbed sample were found to be filled by the dye molecules properly. Thus, the natural dye (*Curcuma Longa sp.*) adsorbed TiO<sub>2</sub> photoanodes could be widely used for the fabrication of efficiently improved DSSC.

## 2. Experimental

### 2.1. Materials

Materials used to produce the TiO<sub>2</sub> films for photoanodes were TiO<sub>2</sub> nanopowder (Degussa P25, USA), indium tin oxide (ITO) coated glass plate (Dyesol, Australia) as substrate materials, Triton X-100, i.e. C<sub>8</sub>H<sub>17</sub>C<sub>6</sub>H<sub>4</sub>(OCH<sub>2</sub>CH<sub>2</sub>)<sub>n</sub>OH (Merck, Germany), titanium IV isopropoxide, i.e. Ti[OCH(CH<sub>3</sub>)<sub>2</sub>]<sub>4</sub>, TTIP (Merck, Germany), polyethylene glycol 6000, i.e. HO(C<sub>2</sub>H<sub>4</sub>O)<sub>n</sub>H, PEG (Merck, Germany), ethanol (BDH, UK), citric acid (C<sub>6</sub>H<sub>8</sub>O<sub>7</sub>, Merck, Germany), acetone (BDH, UK), dye extracted from turmeric (*Curcuma Longa sp.*, local Bangladeshi name holud), etc.

### 2.2. Extraction of natural dye sensitizers

At first, a beaker was washed using distilled water and dried at 60 °C in an oven. Then, the beaker was permitted to be cooled naturally to room temperature (25 °C). Afterwards, 5 g of dry turmeric was dipped in 100 mL of ethanol solvent in a dried beaker to prepare the dye solution. After sealing the beaker top with aluminum foil paper, the beaker was located in a dark place for 12 hours to extract color by self-extraction process [34, 38].

### 2.3. TiO<sub>2</sub> film coating for DSSC photoanode

With help of a glass rod, 1 g of TiO<sub>2</sub> nanopowder (Degussa P25), 1 mL citric acid (0.1 M), 0.2 mL titanium (IV) isopropoxide, 0.05 mL non-ionic surfactant Triton X-100, and 0.1 mL polyethylene glycol were mixed together in a beaker. Then, the mixture of TiO<sub>2</sub> paste was sonicated using an ultrasonic bath for 20 minutes. Two ITO glass substrates each of 1 cm × 1 cm dimension and 10 Ω/cm<sup>2</sup> surface resistance were coated applying the prepared TiO<sub>2</sub> paste by doctor blade method. Then, the ITO glass substrates were annealed at 500 °C for 1 h [34]. Next, the glass substrates were permitted to be cooled slowly for 12 h to room temperature. The thicknesses of the developed TiO<sub>2</sub> films were 10 μm. One of the substrates used as dye free (sample without dye adsorption) was denoted as S1 in the discussion later on. At the next stage, to adsorb the dye molecule, another substrate notated as S2 was immersed into turmeric natural dye beaker for 2 h in a dark place. Then the S2 was cleaned with water and thereafter with ethanol for several times. To get the final phase of the S2 (i.e. dye adsorbed sample), the substrate was dried in natural air for few minutes at room temperature.

### 2.4. XRD characterization

The structural properties and particle size were investigated with an X-ray diffractometer (GBC-EMMA, Australia) from Institute of Fuel Research and Development (IFRD), Bangladesh Council of Scientific & Industrial Research (BCSIR), Dhaka-1205, Bangladesh. At 2θ position, X-ray diffraction technique was applied from 20° to 90°.

### 2.5. SEM characterization

The surface morphologies of the TiO<sub>2</sub> film of the photoanodes were studied by scanning electron microscope (SEM). SEM and EDS studies were performed with a field emission scanning electron microscope (JEOL JSM-7600F, Tokyo, Japan) at the Department of Glass and Ceramic Engineering (GCE), Bangladesh University of Engineering

& Technology (BUET), Dhaka-1000, Bangladesh. During FESEM imaging, the accelerating voltage was maintained at 5 kV to 7 kV to eliminate charging effect.

### 2.6. EDS characterization

Energy dispersive spectroscopy (EDS) is a test to examine the presence of elements through studying the amplitude of X-ray of a wavelength emitted after hitting by electrons that come from electron beam. For the emission of X-ray, the atoms must contain at least K-shell and L-shell where the electron is allowed to dislodge from shell to shell. Therefore, hydrogen, being the only element in the periodic table with only K-shell, is not detectable by EDS. EDS was used to calculate the percentage of various elements existing in the TiO<sub>2</sub> films.

### 2.7. UV-Vis-NIR characterization

The optical properties were studied by UV-Vis-NIR spectroscopy analysis. UV-Vis-NIR spectra of TiO<sub>2</sub> films were taken by UV-Vis-NIR spectrophotometer (Hitachi 4200, Japan) from Institute of Fuel Research and Development (IFRD), Bangladesh Council of Scientific & Industrial Research (BCSIR), Dhaka-1205, Bangladesh. Fresh ITO coated glass substrate was used as a reference.

## 3. Results and discussion

### 3.1. XRD analysis (structural properties)

Using X-ray diffraction technique (from 20° to 90° at 2θ position), crystalline structure of TiO<sub>2</sub> films for dye free (without dye adsorption) (S1) and dye adsorbed samples (S2) were studied. In XRD spectrum, thirteen diffracted peaks for anatase phase A and five peaks for rutile phase R were observed as shown in Fig. 1.

Crystallite size (L): Average crystallite size L of a crystalline structure can be obtained from Scherrer relation [39] given by:

$$L = \frac{k\lambda}{\beta \cos \theta} \quad (1)$$

where λ stands for the wavelength of the incident X-ray CuKα radiation, k for a constant (0.9), β

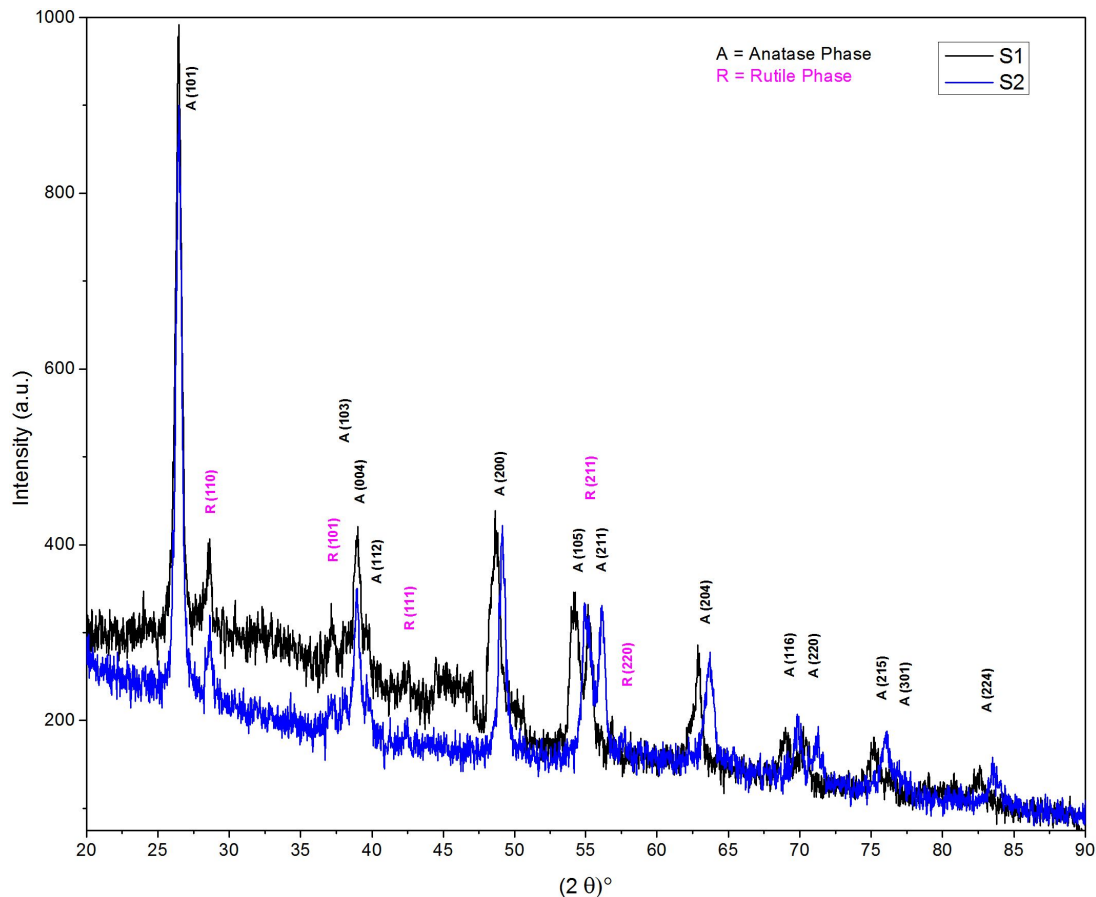


Fig. 1. XRD spectra of TiO<sub>2</sub> films of sample S1 (without dye) and S2 (with dye).

for the full width at half maximum value and  $\theta$  for the Bragg angle of the respective plane peak. XRD results found for different peaks are summarized in Table 1.

**Specific surface area (SSA):** The surface area is an important factor for nanoparticles, because of their large surface-to-volume ratio [40]. There is an inverse relationship between particle size and surface area. The specific surface area (SSA) of the particles, defined as the summation of the areas of exposed surfaces of particles per unit mass [41], derives a value that can be used to determine the type and properties of a material. It has a particular importance in case of adsorption, heterogeneous catalysis and reactions on surfaces [42, 43].

Zhang et al. [44] reported that, the specific surface area and surface to volume ratio increase dramatically as the size of material decreases.

They estimated the high surface area of TiO<sub>2</sub> nanoparticles, which facilitates the reaction/interaction between TiO<sub>2</sub> based devices and the interacting media. Mathematically, specific surface area (SSA) can be calculated from the crystallite size  $L$ , i.e. particle size  $D$  data obtained from XRD analysis by using the following formula [45]:

$$SSA = \frac{6 \times 10^3}{\rho D_p} \quad (2)$$

where  $\rho$  is the density of TiO<sub>2</sub> nanoparticles (4.23 g·cm<sup>-3</sup>),  $D_p$  is the size of the nanoparticle.

The variation of SSA with crystallite size for anatase and rutile phase of TiO<sub>2</sub> is displayed in Fig. 2, which shows the increasing SSA with decreasing crystallite size for both S1 and S2 samples. Therefore, as the particle sizes of the nanoparticles decrease their chemical reactivity increases.

Table 1. Experimental XRD data for anatase A and rutile R phase of nanocrystalline TiO<sub>2</sub> films developed on ITO glass substrate for S1 (without dye) and S2 (with dye) samples.

Phase [A & R]	2(θ)		FWHM [°]		Crystallite size, L [nm]	
	S1	S2	S1	S2	S1	S2
A (101)	26.46	26.56	0.46519	0.19645	17.54	41.55
R (110)	28.64	28.64	0.33672	0.43748	24.35	18.74
R (101)	37.16	38.96	0.4965	0.47626	16.88	17.69
A (103)	37.96	37.94	0.23203	0.3249	36.21	25.86
A (004)	39.02	38.94	0.5192	0.53533	16.23	15.74
A (112)	39.6	39.62	0.33593	0.20059	25.13	42.09
R (111)	42.56	43.52	0.38239	0.07733	22.29	110
A (200)	48.62	49.14	0.82494	0.33587	10.57	26.01
A (105)	54.18	54.92	0.68368	0.19483	13.05	45.95
R (211)	54.42	55.26	0.06868	0.40316	130	22.24
A (211)	55.18	56.16	0.52244	0.15978	17.16	56.35
R (220)	56.86	57.76	0.47222	0.10812	19.13	83.91
A (204)	62.84	63.72	0.40148	0.6603	23.19	14.17

The obtained specific surface area for S1 ranges from 39 m<sup>2</sup>·g<sup>-1</sup> to 134 m<sup>2</sup>·g<sup>-1</sup>, and for S2 from 30 m<sup>2</sup>·g<sup>-1</sup> to 100 m<sup>2</sup>·g<sup>-1</sup>.

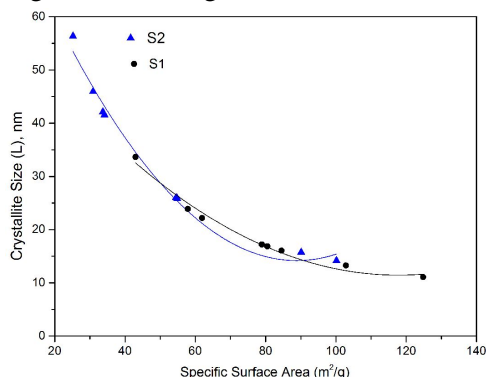


Fig. 2. Variation of crystal size with specific surface area (SSA) for the sample S1 and S2.

Morphology Index (MI): TiO<sub>2</sub> nanopowder is widely used in many diverse applications due to its unique structural, physical and chemical properties. The specific surface area, related to particle morphology and size, influence chemical reactivity of the nanopowder. Morphology index (MI) is calculated from FWHM (full width at half maximum) of XRD peaks by the following equation [46]:

$$MI = \frac{FWHM_h}{FWHM_h + FWHM_p} \quad (3)$$

where MI is the morphology index,  $FWHM_h$  is the highest FWHM value obtained from peaks and  $FWHM_p$  is the particular peak's FWHM for which MI is to be calculated.

The obtained morphology index MI ranges from 0.5 to 0.71 and 0.5 to 0.8 for S1 and S2 sample, respectively. It is correlated with the crystallite size (in the range of 10 nm to 36 nm for S1 and 14 nm to 56 nm for S2 sample) and specific surface area (in the range of 39 m<sup>2</sup>·g<sup>-1</sup> to 134 m<sup>2</sup>·g<sup>-1</sup> for S1 and 30 m<sup>2</sup>·g<sup>-1</sup> to 100 m<sup>2</sup>·g<sup>-1</sup> for S2 sample). The results are presented in Fig. 2 and Fig. 3. It is observed that MI is directly proportional to crystallite size, whereas specific surface area is inversely proportional to particle size. Fig. 3 shows the relationships between MI and crystal size. The observed results for MI confirm the uniformity and fineness of the prepared nanoparticles.

### 3.2. UV-Vis-NIR analysis (optical properties)

Fig. 4 shows the comparison of optical transmittance and absorbance properties of S1 and S2 samples. The measurements were carried out in the wavelength range of 400 nm to 2000 nm. Substrate with dye exhibits significant increase

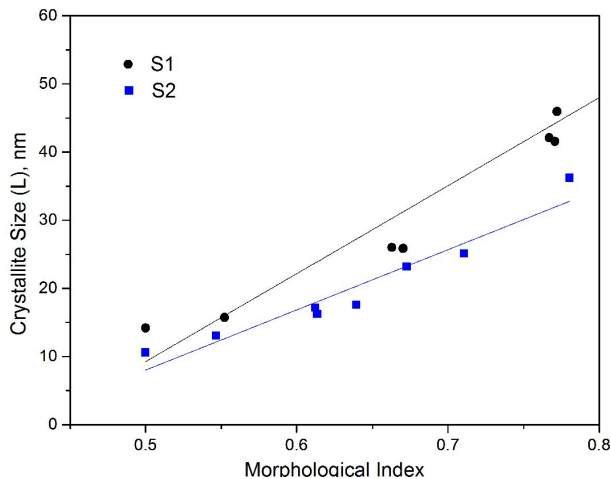


Fig. 3. Variation of crystal size with morphological index (MI) for the samples S1 and S2.

of absorbance and decrease of transmittance within the visible and infrared range compared to the dye free substrate.

### 3.2.1. Absorption coefficient

Absorption coefficient  $\alpha$ , which is related to the characteristics of respective material and wavelength of light, determines the light absorbing properties of a material and can be determined by the relation [47]:  $\alpha = 2.303 A/t$  where  $A$  and  $t$  stand for absorbance and thickness of film, respectively.

### 3.2.2. Optical bandgap

Tauc formula:

$$(\alpha h\nu)^{\frac{1}{n}} = A(h\nu - E_g) \quad (4)$$

relates absorption coefficient  $\alpha$ , energy band  $E_g$  gap, frequency of radiation  $\nu$ , Planck constant  $h$  and a constant  $A$  [48]. The value of  $n$  is different for different types of transition materials. Since  $\text{TiO}_2$  is a direct transition material, hence, the value of  $n$ , in the formula, is taken as 2. To determine the optical band gap,  $(\alpha h\nu)^2$  was plotted against  $h\nu$  as shown in Fig. 5b. Then, extending the linear portion of the curve to the x-axis of  $(\alpha h\nu)^2$  vs.  $h\nu$  plot, optical band gap was estimated as 3.05 eV and 2.85 eV for S1 and S2 sample, respectively. Both samples

(S1 and S2) show wide-bandgaps which values are very close to the ideal bandgap of  $\text{TiO}_2$  of about 3.2 eV [7, 9].

### 3.3. EDS analysis

The EDS graphs of  $\text{TiO}_2$  nanoparticles for S1 are shown in Fig. 6a, Fig. 6b, Fig. 6c and Fig. 6d and for S2 in Fig. 6e, Fig. 6f, Fig. 6g and Fig. 6h. The EDS data were collected from three specified points on the SEM image which were identified by 001, 002 and 003 as shown in Fig. 6a, Fig. 6b and Fig. 6c, respectively, for S1 and Fig. 6f, Fig. 6g and Fig. 6h, respectively, for S2. The atoms were identified by measuring the kinetic energy of the electrons emitted from atoms. The respective kinetic energy for oxygen O and titanium atoms are 0.525 keV and 4.508 keV. Thus, the EDS spectrum of titanium oxide nanoparticles indicates the presence of oxygen and titanium atoms and it also confirms that the produced nanoparticles in the photoanode films are  $\text{TiO}_2$ .

From studying the data in Table 2, it is seen that, the average atomic mass percentage of  $\text{TiO}_2$  obtained from EDX analysis are 68.42 % Ti and 31.58 % O for the dye free sample (S1), and 68.31 % Ti and 31.69 % O for the dye adsorbed sample (S2), which is in agreement with those of the standard value 59.93 % Ti and 40.07 % O in  $\text{TiO}_2$  compound [49]. Thus, it is clear that the produced nanosized particles are  $\text{TiO}_2$ .

### 3.4. SEM analysis (morphological properties)

SEM image is a powerful tool by which surface morphology of nanoparticles can be observed and also size of the particles can be measured. Fig. 7 shows the SEM pictures of the produced  $\text{TiO}_2$  nanoparticles for S1 and S2 samples.

The  $\text{TiO}_2$  nanoparticles that exist in the photoanode film have spherical morphology. Although some particles are found to be agglomerated, most of the particles, termed as primary particles, can be identified in nanometer scale. Typically, agglomeration of nanoparticles may happen for several primary particles. The agglomeration of primary particles is termed as secondary

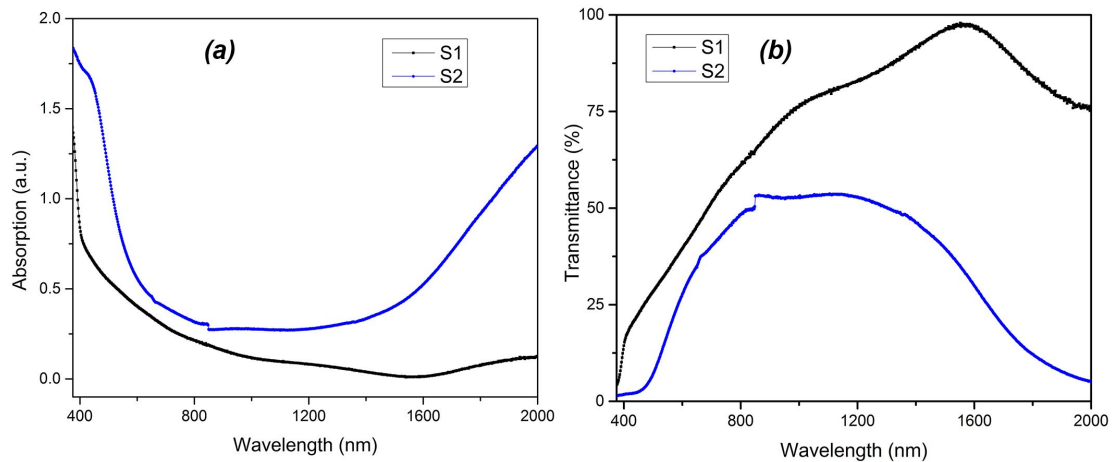


Fig. 4. (a) Transmittance spectrum and (b) absorption spectrum, as a function of wavelength for TiO<sub>2</sub> film of the sample S1 and S2.

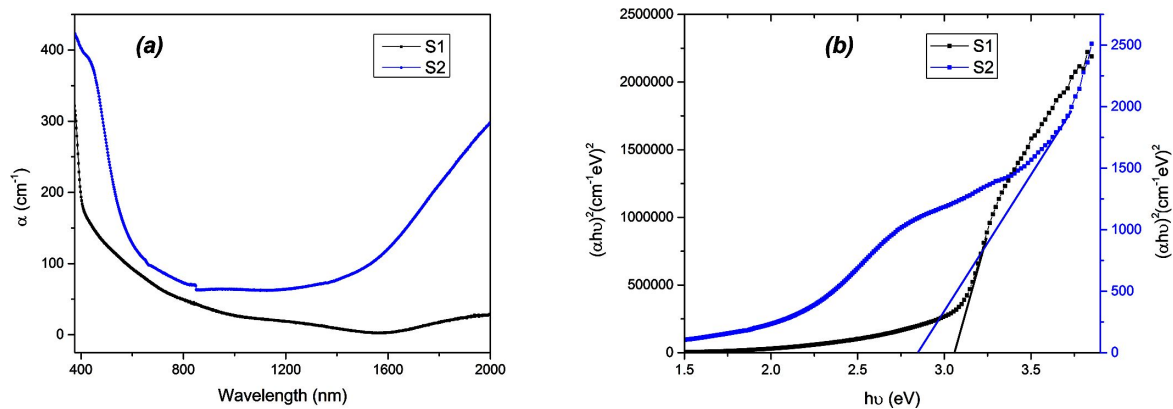


Fig. 5. (a) absorption coefficient and (b) optical bandgap of TiO<sub>2</sub> film for the sample S1 and S2.

particle. They form when the primary particles are held together by weak surface forces (soft agglomeration) such as van der Waals or capillary forces or by strong chemical bonds (hard agglomeration). A significant change is found for the SEM image of the dye adsorbed sample S2. From Fig. 7b, it is observed that most of the mesopores, which are clearly visible in Fig. 7a for sample S1, are filled by dye molecules, which is well agreed with previous reports [34, 38, 50].

#### 4. Conclusions

Since properly dye adsorbed TiO<sub>2</sub> coated photoanode could improve the efficiency of dye-sensitized solar cells, therefore, there is

a significant interest in extensive studies on different characteristics of DSSC photoanodes modified by dye adsorption. In this work, successful analysis of various properties of natural dye adsorbed (*Curcuma Longa sp.*) and dye free TiO<sub>2</sub> coated photoanode layers were carried out. The rate of change in crystallite size against morphological index was found to be lower in the case of dye adsorbed sample. Nonlinearity in crystallite size with specific surface area became higher with adsorbed dye. Light absorption and transmittance capacity changed dramatically in the dye adsorbed sample. Moreover, optical bandgap changed from 3.05 eV to 2.85 eV. SEM investigation confirmed the adsorption of the dye on the nanoporous surface. A comparison of the dye adsorbed and dye

Table 2. Comparison of atomic mass percentages for TiO<sub>2</sub> obtained from EDX with theoretical value for S1 and S2 samples.

Atomic mass [%]	EDX calculation [%]								Theoretical value [%]
	Point 1		Point 2		Point 3		Average		
	S1	S2	S1	S2	S1	S2	S1	S2	
Taitanium (Ti)	67.82	69.82	69.33	69.19	68.11	65.92	68.42	68.31	59.93
Oxygen (O)	32.18	30.18	30.67	30.81	31.89	34.08	31.58	31.69	40.07

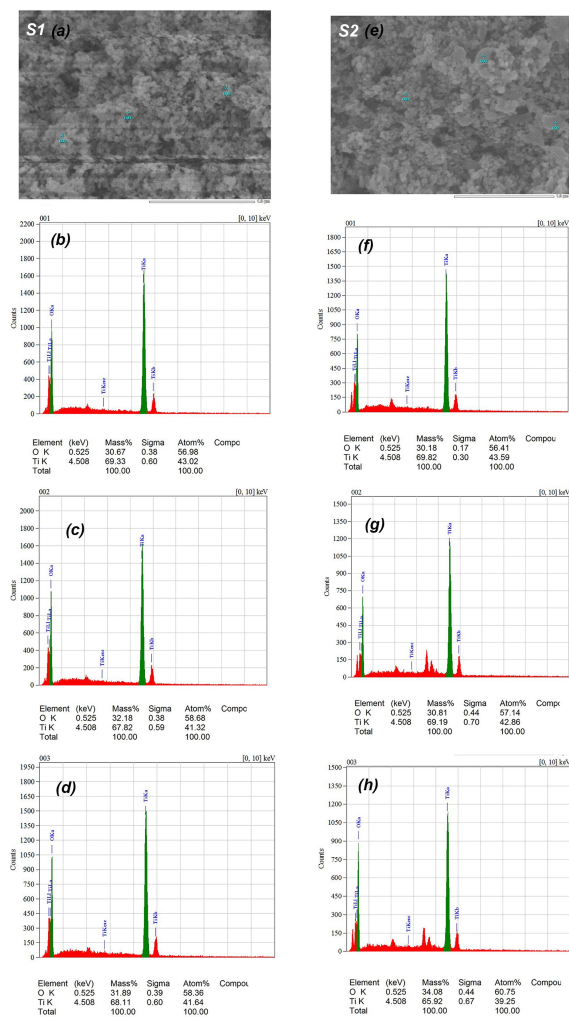


Fig. 6. EDS spectra and distribution of elements for TiO<sub>2</sub> film of S1 (a, b, c, d) and S2 (e, f, g, h) samples.

free samples revealed that, dye affected the optical properties significantly, thereby, slightly influencing the structural and morphological properties of TiO<sub>2</sub> coated photoanode.

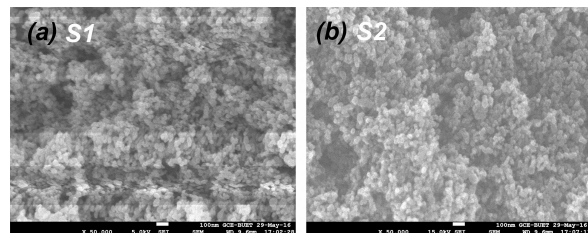


Fig. 7. High resolution SEM images of TiO<sub>2</sub> film for the sample S1 and S2.

## Acknowledgements

The financial grant provided by the Infrastructure Development Comp. Ltd. (IDCOL) and supported by the MOST, Bangladesh. This work was carried out at the Institute of Radiation and Polymer Technology (IRPT), the Atomic Energy Research Establishment, the Bangladesh Atomic Energy Commission.

## References

- [1] GRÄTZEL M., *J. Photoch. Photobio.*, 164 (2004), 3.
- [2] WEI D., AMARATUNGA G., *Int. J. Electrochem. Sc.*, 2 (2007), 897.
- [3] GONÇALVES L.M., BERMUDEZ V.D.Z., RIBEIRO H.A., MENDES A.M., XIAO S., HUANG Y., *Energ. Environ. Sci.*, 1 (2008), 655.
- [4] SOUNDARARAJAN D., YOON J.K., KIM Y.I., KWON J.S., PARK C.W., KIM S.H., *Int. J. Electrochem. Sci.*, 4 (2009), 1628.
- [5] KARAMI H., KABOLI A., *Int. J. Electrochem. Sc.*, 5 (2010), 706.
- [6] GRÄTZEL M., *J. Photoch. Photobio. C*, 4 (2003), 145.
- [7] HARDIN B.E., SNAITH H.J., MCGEHEE M.D., *Nat. Photonics*, 6 (2012), 162.
- [8] SONG W., GONG Y., TIAN J., CAO G., ZHAO H., SUN C., *ACS Appl. Mater. Inter.*, 8 (2016), 13418.
- [9] JASIM K.E., *Dye Sensitized Solar Cells – Working Principles, Challenges and Opportunities*, in: KOSYACHENKO L.A. (Ed.), *Solar Cells – Dye-Sensitized Devices*, InTech, Croatia, 2011, p. 171.
- [10] O'REGAN B., GRÄTZEL M., *Nature*, 353 (1991), 737.
- [11] HAGFELDT A., BOSCHLOO G., SUN L., KLOO L., PETERSSON H., *Chem. Rev.*, 110 (2010), 6595.

- [12] YANG S., KOU H., WANG J., XUE H., HAN H., *J. Phys. Chem. C*, 114 (2010), 4245.
- [13] ROBERTSON N., *Angew. Chem. Int. Edit.*, 45 (2006) 2338.
- [14] GRÄTZEL M., *Prog. Photovoltaics*, 14 (2006), 429
- [15] GLEDHILL S.E., SCOTT B., GREGG B.A., *J. Mater. Res.*, 20 (2005), 3167.
- [16] HAGFELDT A., GRÄTZEL M., *Accounts Chem. Res.*, 33 (2000), 269.
- [17] GRÄTZEL M., *Nature*, 414 (2001), 338.
- [18] GRÄTZEL M., *Nature*, 421 (2003), 586.
- [19] WANG F.M., CHU C.H., LEE C.H., WU J.Y., LEE K.M., TUNG Y.L., *Int. J. Electrochem. Sc.*, 6 (2011), 1100.
- [20] GORLOV M., KLOO L., HAGFELDT A., BOSCHLOO G., KLOO L., GORLOV M., *Dalton T.*, 91 (2008), 2655.
- [21] ARMAND M., ENDRES F., MACFARLANE D.R., OHNO H., SCROSATI B., *Nat. Mater.*, 8 (2009), 621.
- [22] KEMMITT T., AL-SALIM N., WATERLAND M., KENNEDY V., MARKWITZ A., *Curr. Appl. Phys.*, 4 (2004), 189.
- [23] DAHOUDI N.A., ZHANG Q., CAO G., *Int. J. Photoenergy*, 2012 (2012), 1.
- [24] KAKIAGE K., AOYAMA Y., YANO T., OYA K., FUJISAWA J., HANAYA M., *Chem. Commun.*, 51 (2015), 15894.
- [25] KIM S., LEE J.K., KANG S.O., KO J., YUM J.-H., FANTACCI S., ANGELIS F.D., CENSO D.D., NAZEERUDDIN M.K., GRÄTZEL M., *J. Am. Chem. Soc.*, 128 (2006), 16701.
- [26] MATHEW S., YELLA A., GAO P., HUMPHRY-BAKER R., CURCHOD B.F.E., ASHARI-ASTANI N., *Nat. Chem.*, 6 (2014), 242.
- [27] POLO A.S., ITOKAZU M.K., IHA N.Y.M., *Coordin. Chem. Rev.*, 248 (2004), 1343.
- [28] QURRATULAIN, HAMEED S., KAZMI S.A., AHMAD N., KHAN W., *2015 Annu. IEEE India Conf. IEEE*, 2015, p. 1.
- [29] RICHHARIYA G., KUMAR A., TEKASAKUL P., GUPTA B., *Renew. Sust. Energ. Rev.*, 69 (2017), 705.
- [30] WONGCHAREE K., MEEYOO V., CHAVADEJ S., *Sol. Energ. Mat. Sol. C.*, 91 (2007), 566.
- [31] FURUKAWA S., IINO H., IWAMOTO T., KUKITA K., YAMAUCHI S., *Thin Solid Films*, 518 (2009), 526.
- [32] AHMAD M.S., PANDEY A.K., RAHIM N.A., *Renew. Sust. Energ. Rev.*, 77 (2017), 89.
- [33] JOSEPH S., BOBY S.J.M., NATHAN D.M.G.T., SAGAYARAJ P., *Sol. Energ. Mat. Sol. C.*, 165 (2017), 72.
- [34] HOSSAIN M.K., PERVEZ M.F., MIA M.N.H., MORTUZA A.A., RAHAMAN M.S., KARIM M.R., ISLAM J.M.M., AHMED F., KHAN M.A., *Results Phys.*, 7 (2017), 1516.
- [35] SAFIE N.E., LUDIN N.A., SU'AIT M.S., HAMID N.H., SEPEAI S., IBRAHIM M.A., TERIDI M.A.M., *Malaysian J Anal. Sci.*, 19 (2015), 1243.
- [36] BUDDEE S., WONGNAWA S., SRIPRANG P., SRIWONG C., *J. Nanopart. Res.*, 16 (2014), 2336.
- [37] KIM H.-J., KIM D.-J., KARTHICK S.N., HEMALATHA K.V., RAJ C.J., OK S., CHOE Y., *Int. J. Electrochem. Sc.*, 8 (2013), 8320.
- [38] HOSSAIN M.K., PERVEZ M.F., TAYYABA S., UDDIN M.J., MORTUZA A.A., MIA M.N.H., MANIR M.S., KARIM M.R., KHAN M.A., *Mater. Sci.-Poland*, 2017 (Accepted). DOI: 10.1515/msp-2017-0086.
- [39] FARHAT O.F., HALIM M.M., ABDULLAH M.J., ALI M.K.M., ALLAM N.K., *Beilstein J. Nanotech.*, 6 (2015), 720.
- [40] CHEN J., LI Y., WANG Y., YUN J., CAO D., *Mater. Res. Bull.*, 39 (2004), 185.
- [41] AKBARI B., TAVANDASHTI M.P., ZANDRAHIMI M., *Iran. J. Mater. Sci. Eng.*, 8 (2011), 48.
- [42] BAGHERI S., JULKAPLI N.M., HAMID S.B.A., *Sci. World J.*, 2014 (2014), 1.
- [43] IBHADON A., FITZPATRICK P., *Catalysts.*, 3 (2013), 189.
- [44] ZHANG J., XIAO X., NAN J., *J. Hazard. Mater.*, 176 (2010), 617.
- [45] THEIVASANTHI T., ALAGAR M., *Chem. Phys.*, (2013), 1307.
- [46] THEIVASANTHI T., ALAGAR M., *Nano Biomed. Eng.*, 3 (2011), 163.
- [47] CAGLAR M., CAGLAR Y., ILICAN S., *J. Optoelectron. Adv. M.*, 8 (2006), 1410.
- [48] GUPTA R.K., SERBETÇI Z., YAKUPHANOGLU F., *J. Alloy. Compd.*, 515 (2012), 96.
- [49] ConvertUnits website (online): <http://www.convertunits.com/molarmass/TiO2>.
- [50] MIAH M.H., RAHAMAN M.D., SYED I.M., *Bangladesh J. Phys.*, (2015) 1.

Received 2017-05-28

Accepted 2017-10-06